Research Paper

PAIN®

OPEN

Distinct and sex-specific expression of mu opioid receptors in anterior cingulate and somatosensory S1 cortical areas

Maria Zamfir[a,b], Behrang Sharif[a,b,c], Samantha Locke[b,d], Aliza T. Ehrlich[b,e], Nicole E. Ochandarena[f], Grégory Scherrer[f,g,h], Alfredo Ribeiro-da-Silva[b,d], Brigitte L. Kieffer[b,e], Philippe Séguéla[a,b,*]

Abstract

The anterior cingulate cortex (ACC) processes the affective component of pain, whereas the primary somatosensory cortex (S1) is involved in its sensory-discriminative component. Injection of morphine in the ACC has been reported to be analgesic, and endogenous opioids in this area are required for pain relief. Mu opioid receptors (MORs) are expressed in both ACC and S1; however, the identity of MOR-expressing cortical neurons remains unknown. Using the Oprm1-mCherry mouse line, we performed selective patch clamp recordings of MOR+ neurons, as well as immunohistochemistry with validated neuronal markers, to determine the identity and laminar distribution of MOR+ neurons in ACC and S1. We found that the electrophysiological signatures of MOR+ neurons differ significantly between these 2 areas, with interneuron-like firing patterns more frequent in ACC. While MOR+ somatostatin interneurons are more prominent in ACC, MOR+ excitatory neurons and MOR+ parvalbumin interneurons are more prominent in S1. Our results suggest a differential contribution of MOR-mediated modulation to ACC and S1 outputs. We also found that females had a greater density of MOR+ neurons compared with males in both areas. In summary, we conclude that MOR-dependent opioidergic signaling in the cortex displays sexual dimorphisms and likely evolved to meet the distinct function of pain-processing circuits in limbic and sensory cortical areas.

Keywords: Analgesia, Morphine, Pain, Neocortex, GABAergic interneurons, Pyramidal cells, Somatostatin

1. Introduction

Opioids are the most potent and fast-acting analgesics available for acute, postoperative, and chronic pain. In addition to pain alleviation, they have many undesired effects such as tolerance, opioid-induced hypersensitivity, nausea, constipation, respiratory depression, and transition to addiction. The development of highly potent opioids, such as fentanyl, and the overprescription of oxycodone have led to an opioid epidemic.[13,50] Opioids such as morphine can bind to mu opioid receptors (MORs) expressed in pain pathways, including peripheral nerves, spinal cord, and brain.[23,35,47] Opioid actions on peripheral nerves are major contributors to opioid tolerance and opioid-induced hypersensitivity,[14] and their central effects are suggested to dissociate the affective component of pain from its sensory-discriminative component.[24,42,44] Mu opioid receptors are present in the anterior cingulate cortex (ACC) and primary somatosensory cortex (S1).[34,57] The ACC is thought to predominantly contribute to the affective and motivational components of pain.[22,36,45] Moreover, increased binding of endogenous opioids to MOR in the ACC was correlated with decreased affective component of pain.[56] Interestingly, increased binding of endogenous opioids to MOR in S1 was not correlated to a decreased sensory or discriminative perception of pain.[56] Although the role of S1 in nociception has historically been difficult to investigate due its somatotopic organization and pain modulation by attention, the role of S1 in discerning both localization and intensity of noxious stimuli is now widely accepted.[7] The ACC and S1 work together to generate pain experience, as both areas receive information from the medial thalamus and both areas process pain intensity.[11,17]

Mu opioid receptors are Gi/o protein–coupled receptors, and their activation results in neurotransmission inhibition, partly through opening of potassium channels and modulation of voltage-gated calcium channels.[1] Recently, Wang et al.[51] showed that in ACC, MORs are more densely located in the output layer 5. Birdsong and colleagues showed that in the ACC,

Sponsorships or competing interests that may be relevant to content are disclosed at the end of this article.

M. Zamfir and B. Sharif contributed equally to this work.

[a] Department of Neurology and Neurosurgery, Montreal Neurological Institute, McGill University, Montreal, QC, Canada, [b] Alan Edwards Centre for Research on Pain, McGill University, Montreal, QC, Canada, [c] Department of Physiology, McGill University, Montreal, QC, Canada, [d] Department of Pharmacology and Therapeutics, McGill University, Montreal, QC, Canada, [e] Douglas Hospital Research Institute, McGill University, Montreal, QC, Canada, [f] Department of Cell Biology and Physiology The University of North Carolina at Chapel Hill, Chapel Hill, NC, United States, [g] UNC Neuroscience Center The University of North Carolina at Chapel Hill, Chapel Hill, NC, United States, [h] Department of Pharmacology, The University of North Carolina at Chapel Hill, Chapel Hill, NC, United States

**Corresponding author. Address: Montreal Neurological Institute, 3801 University, Suite 778, Montreal, QC H3A 2B4, Canada. Tel.: 1-514-398-5029. E-mail address: philippe.seguela@mcgill.ca (P. Séguéla).*

Supplemental digital content is available for this article. Direct URL citations appear in the printed text and are provided in the HTML and PDF versions of this article on the journal's Web site (www.painjournalonline.com).

PAIN 164 (2023) 703–716

http://dx.doi.org/10.1097/j.pain.0000000000002751

MORs are present on excitatory presynaptic terminals projecting from the medial thalamus into ACC.[3] However, details of the MOR-expressing neuronal subtypes in ACC and S1 remain unknown.

It is becoming increasingly evident that there are sex differences in both pain processing and opioid analgesia.[31,37] Interestingly, research suggests that females require higher levels of morphine compared with males for similar analgesic effects.[32] This could be because of differences in expression of MOR in the central nervous system. Taking advantage of the transgenic Oprm1-mCherry reporter mice,[16] we confirm MOR expression in both excitatory and inhibitory neuronal subtypes and discuss the specific distribution patterns in ACC and S1. Moreover, we found sex-specific differences in the proportion of neurons expressing MOR across layers and cortical areas.

2. Materials and methods

2.1. Contact for reagent and resource sharing

Further information and requests for reagents may be directed to Philippe Séguéla (philippe.seguela@mcgill.ca).

2.2. Experimental model and subject details

All procedures followed the McGill University Animal Care Committee Guidelines. We used the MOR-mCherry (*Oprm1*$^{m\text{-}Cherry/mCherry}$; Jackson Laboratories) reporter mouse line to investigate MOR expression in the cortex.[16] This mouse line was previously validated for normal MOR expression and function in the brain. Multiple lines of evidence at the cellular and behavioral level were provided, including normal transcription levels of the *Oprm1* gene, full agreement between endogenous MOR mRNA and MOR-mCherry regional distribution, normal subcellular localization and trafficking kinetics of MOR-mCherry receptors, normal behavioral responses to morphine and naloxone-induced withdrawal, as well as similar binding density and potency of the MOR agonist DAMGO between *Oprm1*$^{m\text{-}Cherry/mCherry}$ and wild-type animals.[16] Adult *Oprm1*$^{mCherry/mCherry}$ mice, between 2 and 4 months old, were used for all experiments. Male and female mice were used for combined quantification unless otherwise stated. Wild-type C57Bl/6 mice (Charles River Canada, Saint-Constant, QC, Canada) were used as controls for electrophysiology experiments (Supplemental Fig. 1, available at http://links.lww.com/PAIN/B700). *Oprm1*$^{Cre/Cre}$ mice were used for qualitative validation of cellular expression.[37]

2.3. Brain slice preparation and electrophysiology

Animals were deeply anesthetized with systemic Avertin (tribromoethanol, 330 mg/kg, administered by intraperitoneal injection) and perfused transcardially with ice-cold choline chloride–based cutting solution (in mM): 110 choline-Cl, 1.25 NaH_2PO_4, 25 $NaHCO_3$, 7 $MgCl_2$, 0.5 $CaCl_2$, 2.5 KCl, 7 glucose, 3 pyruvic acid, and 1.3 ascorbic acid, with pH and oxygen levels stabilized by bubbling carbogen (O_2 95%, CO_2 5%). Coronal brain sections (300 μm) were cut using a vibratome Leica VT1000S (Richmond Hill, Ontario). The Allen Mouse Brain Atlas was used to determine the location of our regions of interest (Allen Brain Institute, Coronal Sections Version 2, Atlas ID: 1). Sections included the dACC (Bregma +2.345 to 0.845 mm), vACC (+1.145 to 0.845 mm), and S1 (Bregma +1.145 to -0.055 mm), and only one cell from one region was recorded per brain section. Sections were placed in oxygenated (95% O_2, 5% CO_2) extracellular solution (in mM): 125 NaCl, 2.5 KCl, 1.6 $CaCl_2$, 2 $MgCl_2$, 25 $NaHCO_3$, 1.25 NaH_2PO_4, 3 pyruvic acid, 1.3 ascorbic acid, and 10 glucose, pH 7.4. Sections were oxygenated for 1 hour at room temperature before recording. The recording chamber was mounted on the stage of an upright fluorescence microscope Axioskop (Zeiss Canada). In the recording chamber, slices were perfused with the oxygenated standard extracellular solution at ~2 mL/min, and the temperature was maintained at 32°C using a TC-324B temperature controller (Warner Instruments, Hamden, CT). Slices were visualized with an INFINITY 3S-1UR monochrome CCD camera (Teledyne Lumenera, Ottawa, ON) and the INFINITY ANALYZE and CAPTURE software (v6.5.6, Lumenera). Sections were observed using a 4x objective, neurons were selected for recording using a 63x water immersion objective. For recordings in C57Bl/6 mice, the neurons were selected blindly with a bias for selecting pyramidal-like neurons. For recordings in Oprm1-mCherry mice, neurons were selected based on observed fluorescence through a green excitation (G-2A long-pass emission filter). Sections were illuminated with HBO 100 W/2 lamp, powered by Univ Arc Lamp Halogen Power Supply (LEP ltd 990031).

Patch pipettes (5-9 MΩ) were pulled from borosilicate glass (BF150-75-10; Sutter Instruments, Novato, CA) on a Flaming/Brown micropipette puller (Model P-97; Sutter Instruments). The internal solution contained (in mM) 120 K-gluconate, 20 KCl, 2 $MgCl_2$, 0.2 EGTA, 10 HEPES, 7 di-tris phosphocreatine, 4 Na_2-ATP, and 0.3 Na_2-GTP and was adjusted to pH 7.3 with KOH. To visualize the recorded neurons, we used a fixable fluorescent dye Lucifer Yellow (Lucifer Yellow CH; Thermo Fisher Scientific) diluted to [2 mM] into the pipette solution.[21] The osmolarity was verified for both intracellular (pipette solution) and extracellular solutions (~290 and ~300 mOsm, respectively). Giga seals (~2-3 GΩ) were obtained by applying negative pressure on the patch pipette. The series resistance (Rs) was compensated (40%-90%). Data were acquired using an Axopatch 200B amplifier, low-pass filtered at 10 kHz, sampled at 20 kHz using either the Digidata 1322/pClamp 9.2 or the Digidata 1550B/pClamp 11 software setup (Molecular Devices).

In current clamp mode, we injected current ranging from −20 to +140 pA and used a +100 pA square pulse to compare spiking phenotypes. To differentiate between interneuron and pyramidal cells, we analyzed action potential width, action potential after-hyperpolarization (AHP) amplitude, and time to reach AHP. In voltage clamp mode, we gave voltage steps (−60 to −120 mV) (Supplemental Fig. 1, available at http://links.lww.com/PAIN/B700) or held the neuron at −70 mV and observed changes in holding currents associated with GIRK currents. We applied the MOR-selective agonist DAMGO [1 μM] (Cat # 117; Tocris Biosciences) followed by application of the antagonist naloxone hydrochloride [100 μM] (Cat # 599; Tocris Biosciences). We applied the $GABA_B$ agonist baclofen [100 μM] (Cat # ab 120325; Abcam) as a positive control for the presence of GIRK current (Supplemental Fig. 1, available at http://links.lww.com/PAIN/B700). Traces were analyzed offline using Clampfit 11 (Molecular Devices).

2.4. Immunohistochemistry and imaging

Oprm1-mCherry mice were deeply anesthetized with systemic Avertin (tribromoethanol; Sigma-Aldrich) and perfused transcardially with 25 to 50 mL of PBS followed by 100 mL of 4% PFA. Whole brains were extracted, postfixed in 4% PFA overnight at 4°C, and then cryoprotected in 30% sucrose in PBS for 2 days at 4°C. Brains were mounted on the specimen block using O.C.T. Compound (Fisher Scientific). Coronal sections (40 μm) were cut on the cryostat (Leica CM 3050S), and sections spanning our

areas of interest were collected into PBS-filled wells and kept free-floating for immunohistochemistry.

Sections were washed in PBS 3 times for 10 minutes and then blocked for 2 hours at room temperature (RT) with 10% normal donkey serum (Jackson Laboratories) in PBS containing 0.5% Triton X-100 (PBST) to reduce background. Sections were incubated with primary antibodies (**Table 1**), in 3% NDS made with PBS for 48 hours at 4°C on shaker. All sections were treated with anti-mCherry antibody to amplify the MOR-mCherry signal and anti-NeuN to determine neuronal density. SATB2, SOM, VIP, and PV antibodies were applied on separate sections. Sections were then washed in 0.1% PBST, 3 times for 20 minutes. Secondary antibodies (**Table 2**) were applied in 3% NDS made with PBS and incubated for 12 to 24 hours at 4°C on shaker. Sections were then washed in PBS 3 times for 20 minutes and mounted on glass slides (Fisherbrand Superfrost Plus Microscope Slides) using Aqua-Poly/Mount (Polysciences).

For visualization, sections were imaged with a Leica TCS SP8 confocal microscope using ×20 and ×40 objectives. For analysis and quantification purposes, the sections were imaged with a VS-120 Olympus slide scanner under epifluorescence in DAPI, FITC, TRITC, and Cy5 channels using an optical filter set from Semrock (Part Number: DA/FI/TR/Cy5-4X4M-C-000), an Orca r2 Hamamatsu monochrome camera, and an Olympus ×10 objective (Molecular and Cellular Microscopy Platform—Douglas Research Center, Montreal, Canada). Virtual Slide Images (.vsi) files acquired from the slide scanner were opened in FIJI using the BIOP VSI Reader (EPFL, Lausanne, Switzerland) and exported as individual TIFF files for further analysis in FIJI (Image J version 2.1.0).

2.5. Labeling of Oprm1 + neurons with tdTomato

We briefly anesthetized 18- to 19-week-old female *Oprm1*$^{Cre/Cre}$ mice[2] with isoflurane gas and injected with 100 nL of 1.5×10^{12} gc/mL AAV(PHP.eB)-CAG-FLEx-tdTomato (Addgene 28306-PHPeB) in 0.1 M PBS retro-orbitally. We allowed 4 weeks for viral expression before transcardiac perfusion with 30 mL ice-cold 0.1 M PBS followed by 30 mL 4% formaldehyde in 0.1 M PBS. We postfixed brains in 4% formaldehyde in PBS overnight before switching to a 30% sucrose in 0.1 M PBS solution for 48 hours. We cut 40-μm sections using a Leica cryostat and stored slices in glycerol cryoprotectant before mounting and imaging. We imaged sections using a Leica SP8X confocal microscope and adjusted brightness and contrast in FIJI.

2.6. Mouse brain atlas and regional analysis

We used the adult mouse 3D coronal atlas from the Allen Brain Institute (Atlas ID: 602630314). Downloaded svg files through the API were morphed in FIJI to fit each whole brain section using BigWarp.[5,43] We then converted the morphed svg atlas to the region of interest (roi) FIJI file format using the script provided by Nicolas Chiaruttini (**Table 3**). This enabled us to measure the size and boundaries of our areas of interest, as well as analyze individual layers in ACC and S1. We used the cell counter plugin in FIJI and ellipse tool for counting and marking the cells of interest.

Our imaging analysis spanned Bregma +1.745 to −0.055 mm. Rostral dorsal ACC (dACC, 24b) refers to sections spanning Bregma +1.745 to +1.445 mm. We analyzed caudal dACC (24b), ventral ACC (vACC, 24a), and primary somatosensory cortex (S1) from Bregma +1.145 to −0.055 mm. We used "ACC" to refer to the combined data from dACC (24b) and vACC (24a). This combination is supported by a recent suggested nomenclature,[20] which removes the dorsal and ventral division in ACC.

2.7. Quantification and statistical analysis

Statistical analyses were performed with GraphPad Prism 8 and R. We ran paired Student *t* tests, one-way analysis of variance (ANOVA) or two-way ANOVAs, and Wilcoxon signed rank test, with Tukey or Benjamini–Hochberg multiple comparison corrections. Data are presented as mean ± SEM with individual data points. Differences were considered significant when $P < 0.05$. Graphs were generated in GraphPad Prism 8 and R.

3. Results

3.1. Functional cortical mu opioid receptor expression in the Oprm1-mCherry mouse line

We used the Oprm1-mCherry mouse line for both immunohistochemistry and electrophysiology experiments.[16] After amplification of the MOR-mCherry fluorescence signal with anti-mCherry antibodies, we noticed that MORs are distributed throughout the cortical layers of ACC and S1 (**Fig. 1A**). We performed whole-cell patch clamp recording of MOR-mCherry–expressing neurons in acute brain slices (**Figs. 1B and C**). Typically, in the central nervous system, postsynaptic MORs are coupled to G protein–coupled inward rectifying potassium (GIRK) channels.[1] To determine if the MORs were functional in the cortical MOR-mCherry+ neurons, we recorded the current required to maintain the neuron at −70 mV in the absence and presence of MOR agonist. We found that bath application of the selective MOR agonist DAMGO [1 μM] resulted in GIRK channel–mediated increase in holding current in MOR-mCherry+ neurons (+17.24 ± 1.39 pA) but not in MOR-mCherry-negative neurons (−1.82 ± 2.50 pA) ($P < 0.001$). Furthermore, the outward current observed in MOR-mCherry+ neurons was reversed by bath application of the opioid receptor antagonist

Table 1

Primary antibodies.

Primary Ab	Host species	Clonality	Dilution	Company	RRID
Anti-mCherry	Rat	Monoclonal	(1:2000)	Thermo Fisher Scientific	AB_2536611
Anti-NeuN	Guinea pig	Polyclonal	(1:1000)	Millipore	AB_2341095
Anti-SATB2	Rabbit	Polyclonal	(1:2000)	Abcam	AB_2301417
Anti-SOM	Rabbit	Polyclonal	(1:2000)	Peninsula	AB_518614
Anti-PV	Mouse	Monoclonal	(1:5000)	Millipore	AB_2174013
Anti-VIP	Rabbit	Polyclonal	(1:1000)	Immunostar	AB_572270

Table 2

Secondary antibodies.

Secondary Ab	Fluorophore	Dilution	Company	RRID
Donkey anti-rat	Alexa 594	(1:1000)	Thermo Fisher Scientific	AB_2535795
Goat anti-guinea pig	Alexa 647	(1:1000)	Thermo Fisher Scientific	AB_2735091
Donkey anti-mouse	Alexa 488	(1:1000)	Thermo Fisher Scientific	AB_141607
Donkey anti-rabbit	Alexa 488	(1:1000)	Thermo Fisher Scientific	AB_2535792

naloxone [100 μM] (−2.59 ± 5.02 pA) ($P < 0.01$) (**Figs. 1D and E**). Naloxone did not significantly alter the holding current in MOR-mCherry-negative cells (−3.17 ± 2.63 pA) ($P > 0.05$). These results confirm that MORs are functionally expressed on cortical MOR-mCherry+ neurons in the *Oprm1*$^{mCherry/mCherry}$ line. We performed similar voltage clamp recordings in wild-type C57Bl/6 mice and found that bath application of DAMGO induced a GIRK current in 13% of excitatory pyramidal cells (2 of 15 neurons) (Supplemental Fig. 1, available at http://links.lww.com/PAIN/B700). By comparing MOR-mCherry+ and MOR-mCherry-negative neurons within ACC, we found significant differences in spiking properties, with MOR-mCherry+ neurons more often displayed interneuron-like firing, whereas MOR-mCherry-negative neurons more often showed pyramidal neuron-like firing (Supplemental Fig. 2, available at http://links.lww.com/PAIN/B700).

3.2. Differences in firing pattern properties of mu opioid receptor-mCherry+ neurons in anterior cingulate cortex and S1

We next examined the firing patterns of neurons recorded in ACC and S1. We recorded primarily layer 5 neurons, the precise locations of which are indicated in **Figure 2A**. We recorded MOR-mCherry+ neurons with interneuron-like firing pattern (blue circles) and excitatory or pyramidal-like firing patterns (green triangles). All ACC MOR-mCherry+ neurons had interneuron-like firing pattern (**Fig. 2B**), whereas the S1 MOR-mCherry+ neurons had both interneuron-like firing pattern (n = 2) and pyramidal-like firing patterns (n = 8) (**Fig. 2C**). To further analyze these firing properties, we measured the AHP amplitude and time to reach AHP (**Figs. 2D and E**). The ACC MOR-mCherry+ neurons had larger AHP amplitudes (13.54 ± 0.89 mV) compared with S1 MOR-mCherry+ neurons (7.50 ± 1.73 mV) ($P < 0.01$) (**Fig. 2F**).

Table 3

Reagents and resources.

Reagent or resource	Source	Identifier
Chemicals		
DAMGO	Tocris Biosciences	Cat # 117/1
Naloxone	Tocris Biosciences	Cat # 0599/100
Baclofen	Abcam	Cat # ab 120325
Lucifer Yellow CH, potassium salt	Thermo Fisher Scientific	Cat # L1177
Tribromoethanol (Avertin)	Sigma-Aldrich	Cat # T48402
2-Methyl-2-butanol	Sigma-Aldrich	Cat # 240486
Experimental models: organisms/strains		
Oprm1$^{mCherry/mCherry}$ mice	Jackson Laboratories	Stock no: 007559
C57Bl/6 mice	Charles River Laboratories	Strain code: 027
Software and algorithms		
FIJI—Image J	https://imagej.net/Fiji	Version 2.1.0
BIOP VSI reader—FIJI	https://www.epfl.ch/research/facilities/ptbiop/	NA
BigWarp plugin—FIJI	https://imagej.net/BigWarp	NA
Allen Brain Atlas—adult mouse, 3D coronal atlas	http://atlas.brain-map.org/atlas?atlas=1 - atlas=1&plate=100960340&structure=549&x=5280&y=3743.999989827474&zoom=-3&resolution=13.96&z=5 https://community.brain-map.org/t/how-do-i-download-reference-atlas-images/94	Atlas ID: 602630314 Version 3 (2015-17)
Allen Brain Atlas—adult mouse, 3D coronal atlas	http://mouse.brain-map.org/experiment/thumbnails/100048576?image_type=atlas	Atlas ID: 1 Version 2 (2011)
SVG to ROI groovy script by Nicolas Chiaruttini, PhD	https://gist.github.com/NicoKiaru/ae00117cd6d33fea500d2867a5e669d9	NA
pClamp 9/10.7/11	Molecular devices	NA
Clampfit 10.7		
Prism 8	Graphpad	NA
Affinity Designer	Serif Europe	NA
Excel 2016	Microsoft	NA
R	https://www.r-project.org/	NA

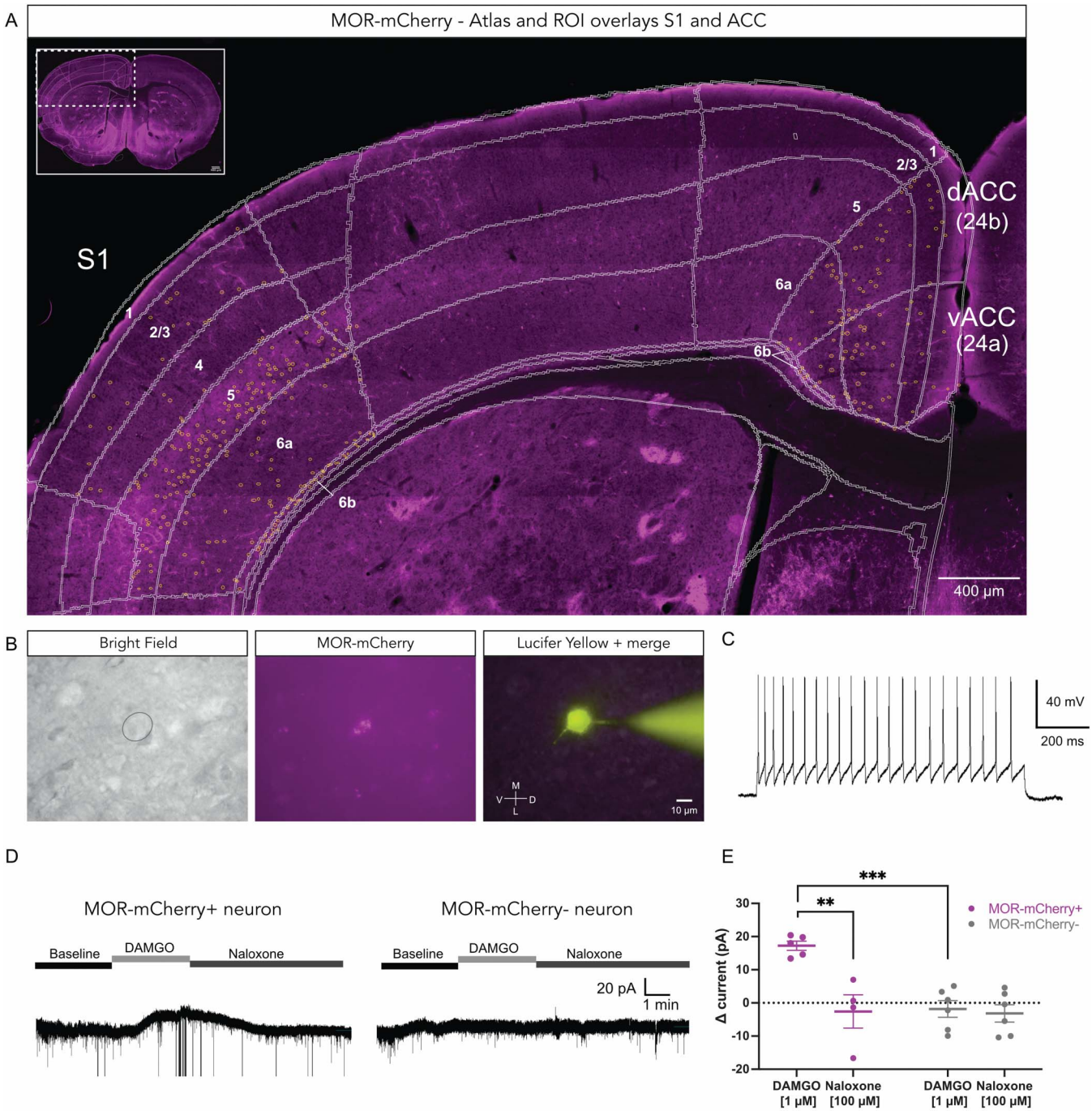

Figure 1. Functional MORs expressed in MOR-mCherry-expressing neurons. (A) Representative MOR-mCherry expression in the adult mouse cortex. Anti-mCherry staining was used to amplify the MOR-mCherry fluorescence signal. Mouse brain atlas is overlaid in white, and yellow circles outline MOR-mCherry+ neurons. (B) Identification of MOR-mCherry-expressing neuron electrophysiological recording set up at ×63 magnification. Bright field view (left panel), direct nonamplified MOR-mCherry signal (middle panel), recorded neuron, and pipette filled with Lucifer Yellow CH (right panel). (C) Typical firing pattern of a MOR-mCherry+ neuron in ACC in response to injection of +100 pA pulse current. (D) Typical voltage clamp recording traces at Vh = −70 mV for MOR-mCherry+ neuron (left) and MOR-mCherry-negative neuron (right) at baseline, during bath application of DAMGO [1 µM] and naloxone [100 µM]. (E) Quantification of differential holding current (drug minus baseline current) in MOR-mCherry+ neurons (n = 5 cells, 4 mice) and MOR-mCherry-negative neurons (n = 6 cells, 3 mice). Recordings were performed in male mice. Two-way mixed ANOVA, $F(1,17) = 10.07$, $P = 0.0056$. Tukey posthoc. Data are presented as mean ± SEM, with dots showing individual neurons, $^{**}P < 0.01$, $^{***}P < 0.001$. MORs, mu opioid receptors.

The time to reach the AHP was shorter in ACC MOR-mCherry+ neurons (4.10 ± 0.26 ms) compared with S1 MOR-mCherry+ neurons (12.11 ± 1.91 ms) ($P < 0.0001$) (**Fig. 2G**). Interestingly, other electrophysiological properties including firing frequency, input resistance, and cell capacitance were not significantly different between ACC and S1 MOR-mCherry+ neurons (Supplemental Fig. 3, available at http://links.lww.com/PAIN/B700). These results suggest that MORs are expressed by both inhibitory and excitatory neurons in the cortex and in different proportions in different cortical areas. Our data also suggest that in layer 5, there are more excitatory MOR-mCherry+ neurons present in S1 compared with ACC (**Figs. 2H and I**). We note that in the electrophysiology preparation, without amplification of the MOR-mCherry signal, only the brightest MOR-mCherry+ neurons were

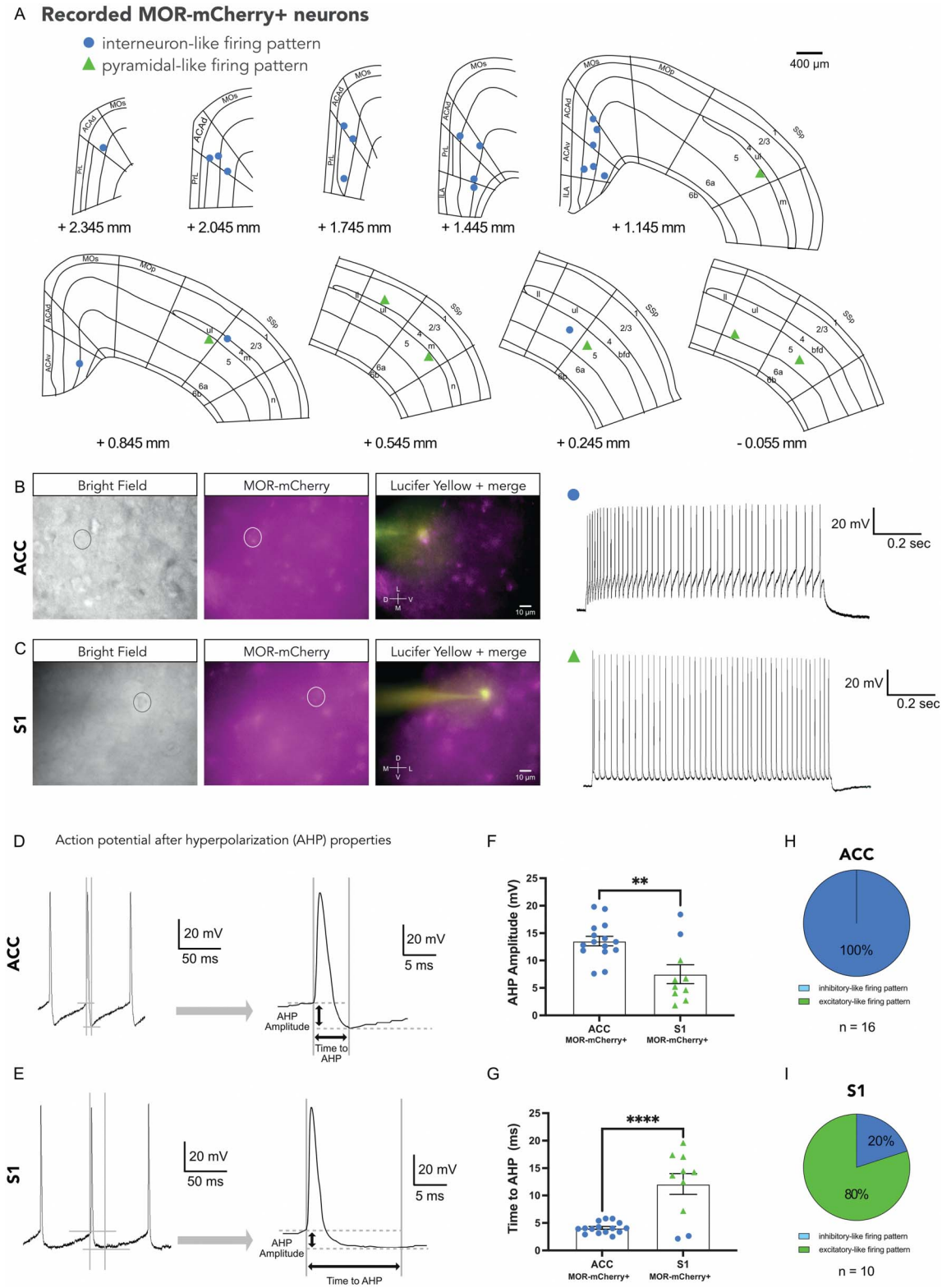

Figure 2. Distinct electrophysiological properties of MOR-mCherry+ neurons in ACC and S1. (A) Mouse brain atlas showing location of recorded MOR-mCherry+ neurons. (B) Representative images of MOR-mCherry tissue in bright field view (left panel), MOR-mCherry signal (middle panel), recorded neuron, and pipette (right panel). Visualization and current clamp trace of a MOR-mCherry+ neuron in ACC in response to 100 pA current pulse. (C) Visualization and current clamp trace of MOR-mCherry+ neuron in S1 in response to 100 pA current pulse. (D) Typical action potential properties, specifically after-hyperpolarization potential (AHP) amplitude, and time to AHP measured from action potential initiation point, in MOR-mCherry+ interneuron-like in ACC, and (E) in MOR-mCherry+ pyramidal-like firing pattern in S1. (F) Quantification of AHP amplitude. In ACC, MOR-mCherry+ neurons have significantly larger AHP (13.54 ± 0.89 mV) compared with S1 (7.50 ± 1.73 mV), $t(23) = 3.399$, $P = 0.0025$. (G) Quantification of time to AHP. In ACC, times to AHP of MOR-mCherry+ (4.10 ± 0.26 ms) are shorter compared with S1 (12.11 ± 1.91 ms), $t(23) = 5.073$, $P < 0.0001$. ACC MOR-mCherry+ group (n = 16 cells, 10 mice) and S1 MOR-mCherry+ group (n = 10 cells, 7 mice). Recordings were performed in male mice. Proportions of inhibitory and excitatory neuron firing patterns in ACC (H) and S1 (I). Data are presented as mean ± SEM with dots show individual neurons, $^{**}P < 0.01$; $^{****}P < 0.0001$. MORs, mu opioid receptors.

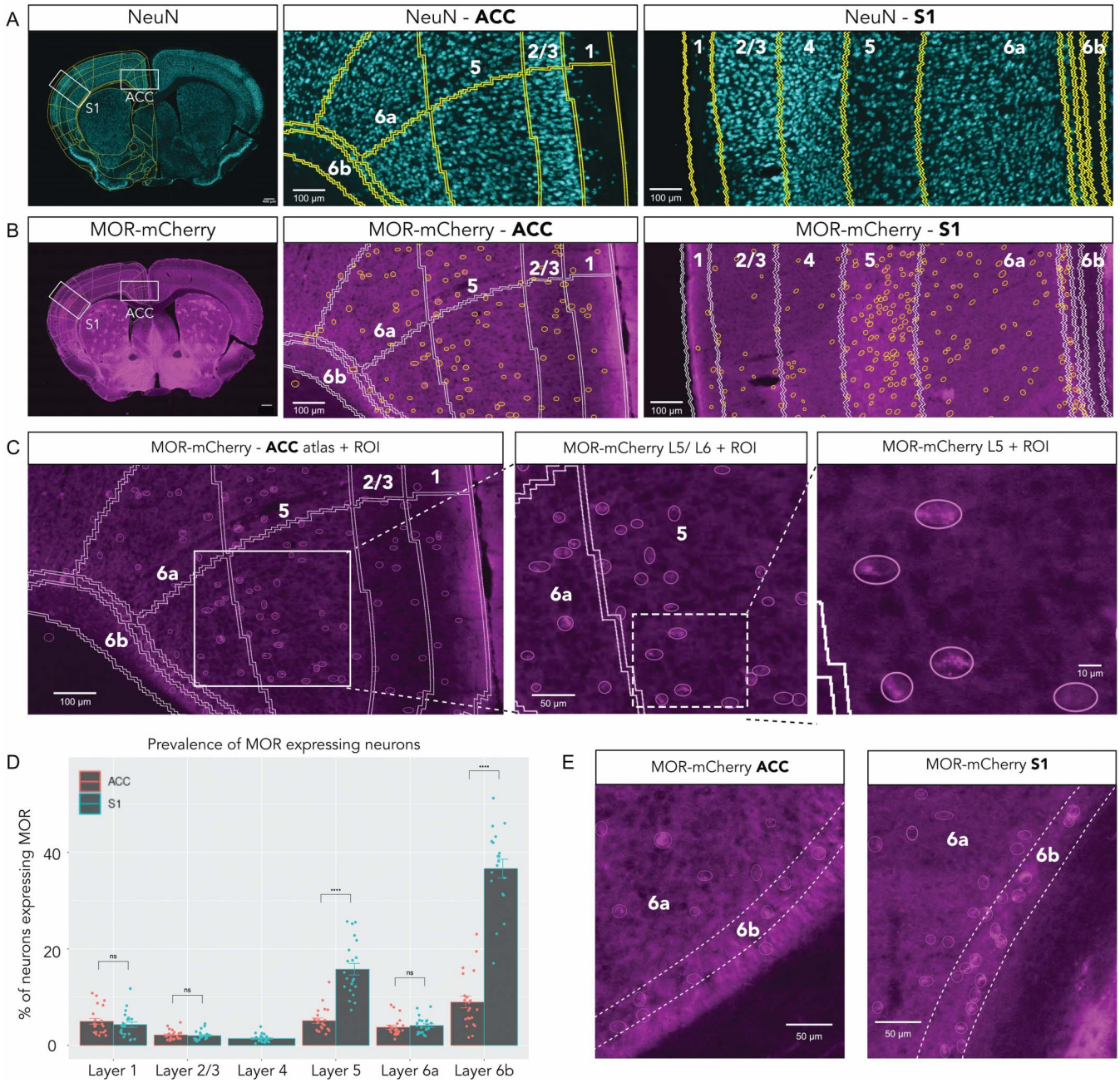

Figure 3. Differences in MOR-mCherry expression pattern between ACC and S1. (A) NeuN pan-neuronal staining of whole mouse brain (left), ACC (middle), and S1 (right). Mouse brain atlas is overlaid. (B) MOR-mCherry expression using anti-mCherry staining of whole mouse brain (left), ACC (middle), and S1 (right). Atlas overlay in white. Yellow circles are outlining MOR-mCherry+ neurons. (C) Increasing magnifications of MOR-mCherry staining showing the MOR-mCherry+ neuron selection process. (D) Quantification of MOR-mCherry+ neurons over total number of neurons. Two-way mixed ANOVA $F(1.98, 35.66) = 191.38$, $P < 0.0001$. Pairwise comparisons using Wilcoxon signed rank test. (E) Typical MOR-mCherry staining in ACC L6b (left) and S1 L6b (right). Pooled male group (n = 12 sections, 3 mice) and female group (n = 10 sections, 3 mice). Data are presented as mean ± SEM, with dots showing individual data points, ****$P < 0.0001$. MORs, mu opioid receptors.

visible and thus selected for recording. Because of this limitation, we performed further immunohistochemistry experiments to investigate MOR expression in ACC and S1.

3.3. Distribution of mu opioid receptor–expressing neurons in anterior cingulate cortex and S1 by layer

To determine and compare the density of MOR-expressing neurons in ACC and S1, we used an anti-NeuN antibody to stain for cortical neurons (**Fig. 3A**). Differences in neuronal density (Supplemental Fig. 4, available at http://links.lww.com/PAIN/B700) are normalized for the remainder of the data presented. We analyzed the amplified MOR-mCherry signal in each cortical area and layer (**Figs. 3B and C**).

We found that the percentage of MOR-mCherry+ neurons varied both by layer and by cortical area, ranging from ~1.4% up to ~37% of total neurons. In our analysis, we covered a range of rostral sections where dACC is present without vACC or S1 (Bregma +1.745 to +1.445 mm). We found that MOR-mCherry density was not significantly different within dACC (24b) along its rostro-caudal axis (Bregma +1.145 to −0.055 mm) (Supplemental Fig. 5, available at http://links.lww.com/PAIN/B700). We also found

that MOR-mCherry density was not significantly different between dACC (24b) and vACC (24a) when comparing within layers (Supplemental Fig. 6, available at http://links.lww.com/PAIN/B700). Given these results, we grouped dACC and vACC into "ACC" for the remainder of this study.

In ACC, MOR-mCherry expression was the highest in L6b (9.0% of total neurons ± 1.2%) and the lowest in L2/3 (2.2% of total neurons ± 0.2%). In S1, MOR-mCherry expression was the highest in L6b (37.1% of total neurons ± 1.8%) and the lowest in L4 (1.4% of total neurons ± 0.2%). MOR-mCherry expression in S1 L5 was significantly higher compared with ACC L5 (15.8% ± 1.2% vs 5.1% ± 0.5%, respectively) ($P < 0.0001$) (**Fig. 3E**). Furthermore, MOR-mCherry expression in S1 L6b was significantly higher compared with ACC L6b (37.1% ± 1.8% vs 9.0% ± 1.2%, respectively) ($P < 0.0001$) (**Fig. 3E**). MOR-mCherry expression was not significantly different between ACC and S1 for L1, L2/3, and L6a.

To further validate the MOR expression pattern found in the *Oprm1*$^{mCherry/mCherry}$ mouse line, we took advantage of the adeno-associated virus capsid PHP.eB, which allows infection and labeling of neurons throughout the CNS after intravenous administration.[8] To selectively label *Oprm1*+ neurons, we injected PHP.eB-CAG-FLEx-tdTomato in the *Oprm1*$^{Cre/Cre}$ mice.[2] Supplementary Figure 7 (available at http://links.lww.com/PAIN/B700) shows that the cortical distribution of tdTomato in ACC and S1 of *Oprm1*$^{Cre/Cre}$ mice was remarkably similar to that of MOR-mCherry. Specifically, tdTomato labeled multiple populations of inhibitory neurons and excitatory neurons, recognized based on their characteristic morphologies, throughout cortical layers 1-6b. These cortical neurons notably include the L6b and S1 L5 pyramidal neuron populations observed in the *Oprm1*$^{mCherry/mCherry}$ mouse line.

3.4. Larger proportion of excitatory mu opioid receptor neurons in S1 compared with anterior cingulate cortex

To further investigate the neuronal populations expressing MOR, we first analyzed the co-expression of MOR-mCherry with SATB2, a transcription factor and selective marker of excitatory cortical neurons (**Fig. 4A**).[6,28] We found that the percentage of MOR-mCherry+ neurons that co-express SATB2 ranged from ~24% to ~81%, varying by both layer and cortical area (**Fig. 4B**). In ACC, MOR-mCherry/SATB2 co-expression was highest in L6b (81.0% ± 7.5%) and lowest in L1 (24.2% ± 5.3%). Similarly, in S1, MOR-mCherry/SATB2 co-expression was highest in L6b (81.4% ± 9.3%) and lowest in L1 (26.4% ± 15.9%). Interestingly, MOR-mCherry/SATB2 co-expression was significantly higher in S1 L5 compared with ACC L5 (68.6% ± 2.7% vs 31.3% ± 5.7%, respectively, $P < 0.01$). In addition, MOR-mCherry/SATB2 co-expression was significantly higher in S1 L6a compared with ACC L6a (53.9% ± 2.2% vs 33.6% ± 3.2%, respectively, $P < 0.01$). MOR-mCherry/SATB2 co-expression was not significantly different between ACC and S1 for L1, L2/3, and L6b.

3.5. Larger proportion of SOM+ mu opioid receptor interneurons in anterior cingulate cortex compared with S1

To establish which type(s) of GABAergic interneuron(s) express MOR in ACC and S1, we determined MOR-mCherry co-expression with somatostatin (SOM), parvalbumin (PV), and vasoactive intestinal peptide (VIP). We found that the percentage of MOR-mCherry neurons that were SOM+ ranged from 0% to ~53%, varying by layer and cortical area (**Figs. 4C and D**). In ACC, MOR-mCherry/SOM co-expression was highest in L5 (53.8% ± 8.3%) and lowest in L6b (10.3% ± 2.8%). However, in S1, MOR-mCherry/SOM co-expression was highest in L6a (47.2% ± 5.6%) and lowest in L1 (0%). Interestingly, MOR-mCherry/SOM co-expression was significantly higher in ACC compared with S1 for L1, L2/3, and L5: ACC L1 vs S1 L1 (30.7% ± 5.3% and 0, respectively, $P < 0.01$), ACC L2/3 vs S1 L2/3 (36.2% ± 5.7% and 12.1% ± 1.4%, respectively, $P < 0.01$), and ACC L5 vs S1 L5 (53.8% ± 8.3% and 12.9% ± 1.7%, respectively, $P < 0.01$). MOR-mCherry/SOM co-expression was not significantly different between ACC and S1 for L6a and L6b.

3.6. Mu opioid receptor/PV and mu opioid receptor/vasoactive intestinal peptide co-expression in anterior cingulate cortex compared with S1

We found that the percentage of MOR-mCherry neurons that were PV+ ranged from ~0 to ~21%, varying by layer (**Figs. 4E and F**). Interestingly, MOR-mCherry/PV co-expression follows similar trend in ACC and S1. For both ACC and S1, the highest co-MOR-mCherry/PV co-expression was found in L2/3 (ACC L2/3-14.6% ± 4.6% and S1 L2/3 21% ± 3.4%). Similarly, for both ACC and S1, the lowest MOR-mCherry/PV co-expression level was in L1 & L6b, where 0% of MOR-mCherry+ neurons express PV. However, MOR-mCherry/PV co-expression was significantly higher in S1 L5 (13.8% ± 1.5%) compared with ACC L5 (6.8% ± 1%) ($P < 0.05$). MOR-mCherry/PV co-expression was not significantly different between ACC and S1 for all other layers.

We found that the percentage of VIP+ neurons ranged from ~1.3% to ~13% of MOR-mCherry+ neurons, varying by layer (**Figs. 4G and H**). Interestingly, MOR-mCherry/VIP co-expression was not significantly different between ACC and S1 for all layers.

3.7. Expression patterns of SATB2, SOM, parvalbumin, and vasoactive intestinal peptide in anterior cingulate cortex and S1

Next, to quantitate the proportions of MOR-mCherry+ neurons in each neuronal population in ACC and S1, we analyzed the expression patterns of SATB2, SOM, PV, and VIP.

In ACC, SATB2 expression was highest in L6b (89% of total neurons ± 3.2%) and lowest in L1 (31.2% ± 3.2%) (**Fig. 5** A i). Similarly, in S1, SATB2 expression was highest in L6b (96.9% ± 7.4%) and lowest in L1 (36.4% ± 4.1%). There were no significant differences in SATB2 expression between ACC and S1 for all layers ($P > 0.05$). We found that in ACC, SATB2/MOR-mCherry co-expressing neurons were evenly distributed throughout L2/3, L5, L6a, and L6b. Whereas for S1, SATB2/MOR-mCherry co-expressing neurons were more densely located in L5 and L6b (**Fig. 5B**).

In ACC, SOM expression was highest in L5 (6.7% of total neurons ± 0.6%) and lowest in L6b (1.7% ± 0.8%) (**Fig. 5A ii**). In S1, SOM expression was highest in L5 (10% ± 0.5%) and lowest in L1 (0.5% ± 0.2%). SOM expression was significantly higher in ACC L1 compared with S1 L1 (5.6% ± 1% and 0.5%± 0.2%, respectively, $P < 0.05$), and in ACC L2/3 compared with S1 L2/3 (3% ± 0.2% and 2.4% ± 0.1%, respectively, $P < 0.05$). Conversely, SOM expression in S1 L5 was significantly higher vs ACC L5 (10% ± 0.5% and 6.7% ± 0.6%, respectively, $P < 0.01$). We found that for both ACC and S1, SOM/MOR-mCherry co-expressing interneurons were more densely located in L5 and L6a (**Fig. 5C**).

In ACC, PV expression was highest in L5 (6.7% of total neurons ± 0.5%) and lowest in L6b (0.3% ± 0.2%) (**Fig. 5A** iii). In S1, PV expression was highest in L5 (13.8% ± 1.2%) and lowest in L1

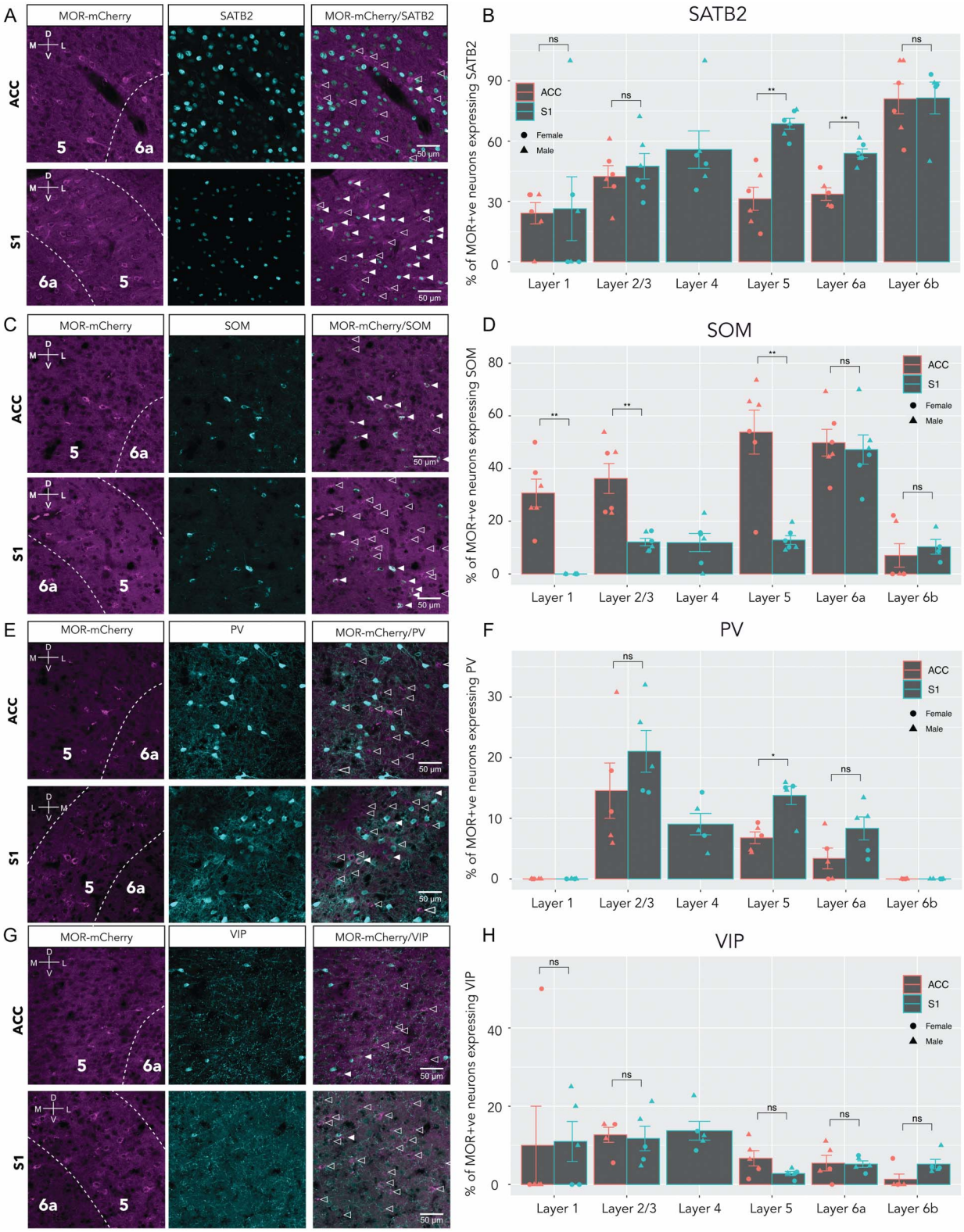

Figure 4. Regional and layer-specific expression of MOR in excitatory and inhibitory neuronal subsets. (A) Representative confocal images of ACC (top row) and S1 (bottom row), with anti-mCherry staining (left), anti-SATB2 (middle), and merge (right). Filled arrowheads indicate co-expression of MOR-mCherry and SATB2. Empty arrowheads indicate MOR-mCherry-only expressing neurons for all panels. (B) Quantification of SATB2 staining in ACC and S1. Two-way mixed ANOVA $F(4,16) = 1.47$, $P = 0.26$. Pairwise comparisons using Wilcoxon signed rank test. (C) Representative images of SOM and MOR-mCherry staining; filled arrowheads indicate MOR-mCherry/SOM co-expression. (D) Quantification of SOM staining in ACC and S1. Two-way mixed ANOVA $F(4,12) = 3.79$, $P = 0.032$. Wilcoxon signed rank test. (E) Sample images of PV staining; filled arrowheads indicate MOR-mCherry/PV co-expression. (F) Quantification, two-way mixed ANOVA $F(4,16) = 1.07$, $P = 0.4$. Wilcoxon signed rank test. (G) Sample images of VIP staining; filled arrowheads indicate MOR-mCherry/VIP co-expression. (H) Quantification, two-way mixed ANOVA $F(1.16, 4.63) = 0.2$, $P = 0.71$. For each (B), (D), (F), and (H) male groups (n = 3 sections, 3 mice) female groups (n = 2 or 3 sections, 3 mice). Data are presented as mean ± SEM, with dots showing individual data points; females are shown with circles and males with triangles. $^{*}P < 0.05$, $^{**}P < 0.01$. MORs, mu opioid receptors.

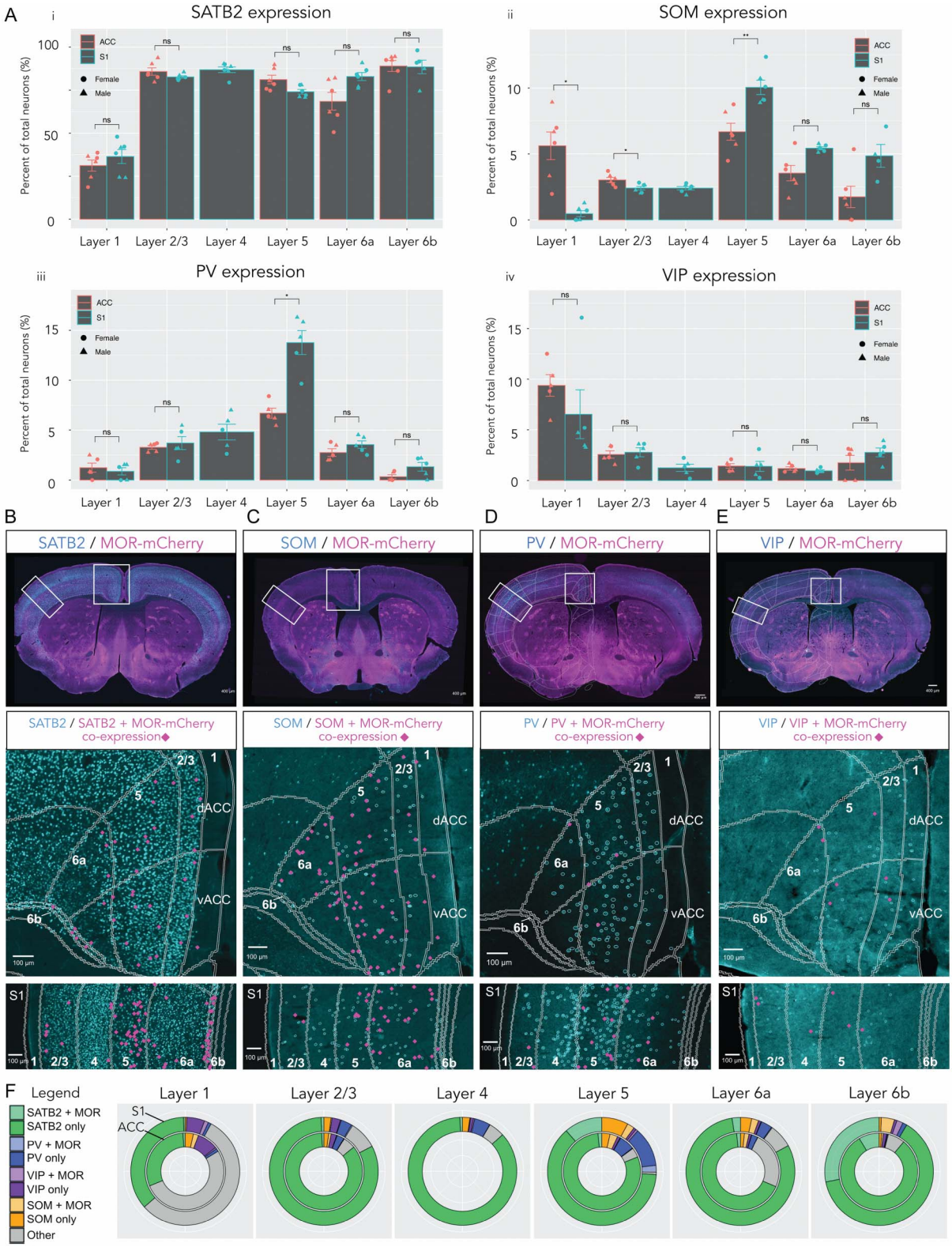

Figure 5. Distribution of excitatory and inhibitory neuronal markers and co-expression with MOR in ACC and S1. (A) i) Quantification of SATB2 staining. Two-way mixed ANOVA $F(4,16) = 4.38$, $P = 0.014$. Wilcoxon signed rank test. ii) Quantification for SOM staining. Two-way mixed ANOVA $F(4,12) = 22.91$, $P < 0.0001$. Wilcoxon signed rank test. iii) Quantification for PV staining. Two-way mixed ANOVA $F(4,16) = 14.83$, $P < 0.0001$. Wilcoxon signed rank test. iv) Quantification for VIP staining. Two-way mixed ANOVA $F(4,16) = 2.93$, $P = 0.054$. Wilcoxon signed rank test. For each i), ii), iii), iv), male groups (n = 3 sections, 3 mice) and female groups (n = 2 or 3 sections, 3 mice). Data are presented as mean ± SEM, with dots showing individual data points, females shown with circles and males with triangles. (B) Top panel: sample whole brain image merge of SATB2 staining (cyan) and MOR-mCherry (magenta). Distribution of SATB2/MOR-mCherry co-expression in ACC and S1 (middle and lower panel, respectively). Pink markers are showing location of SATB2+ neurons that co-express MOR-mCherry. (C) SOM and MOR-mCherry staining and their co-expression. (D) PV and MOR-mCherry staining and their co-expression. (E) VIP and MOR-mCherry staining and their co-expression. (F) Nested pie charts showing prevalence of markers (SATB2, SOM, PV, and VIP) by layer. ACC is represented by the inner ring and S1 by the outer ring. MOR-mCherry co-expression is specified in lighter shades of each marker colour. $^{*}P < 0.05$, $^{**}P < 0.01$, $^{***}P < 0.001$. MORs, mu opioid receptors.

(0.9% ± 0.4%). Parvalbumin expression was significantly higher in S1 L5 compared with ACC L5 (13.8% ± 1.2% and 6.7% ± 0.5%, respectively, $P < 0.05$) (**Fig. 5C** ii). Parvalbumin expression was not significantly different between ACC and S1 for all other layers ($P > 0.05$). We found that for both ACC and S1, PV/MOR-mCherry co-expressing interneurons were more densely located in L5 and L6a (**Fig. 5D**).

In ACC, VIP expression was highest in L1 (9.4% of total neurons ± 1.1%) and lowest in L6a (1.2% ± 0.2%). Similarly, in S1, VIP expression was highest in L1 (6.5% ± 2.4%) and lowest in L6a (1% ± 0.1%) (**Fig. 5A** iv). Vasoactive intestinal peptide expression was not significantly different between ACC and S1 all layers ($P > 0.05$). We found that VIP/MOR-mCherry co-expressing interneurons were more densely located in L2/3, L5, and L6a as opposed to L1 and L6b (**Fig. 5E**). We generated nested pie charts to facilitate the dual comparison of marker expression and MOR-mCherry co-expression in ACC (inner ring) and S1 (outer ring) (**Fig. 5F**).

3.8. Higher expression of mu opioid receptor in females vs males

We then compared MOR-mCherry expression in ACC and S1 of female vs male mice (**Fig. 6**). For S1, the greatest sex difference was found in L5, where females had significantly higher proportion of MOR-mCherry+ neurons (20.7% of total neurons ± 1.3%) than males (11.6% ± 0.7%) ($P < 0.001$) (**Fig. 6C**).

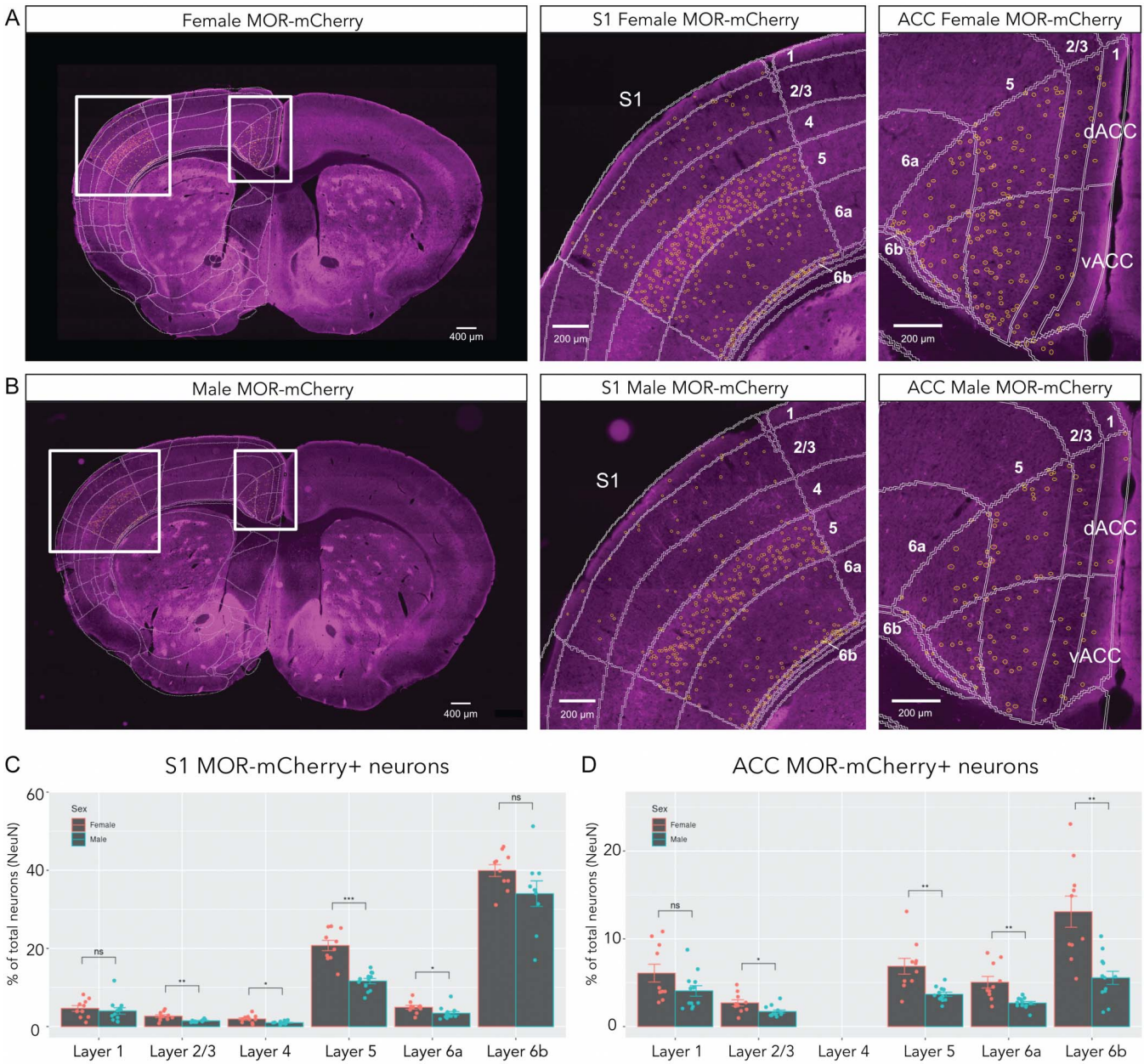

Figure 6. Sex differences in MOR expression between ACC and S1. (A) Representative images from a female MOR-mCherry mouse, whole brain (left), higher magnification of S1 (middle), and ACC (right) areas. Mouse brain atlas overlaid in white, and MOR-mCherry ROIs shown as yellow circles. (B) Representative images from a male MOR-mCherry mouse, whole brain (left), S1 (middle), and ACC (right). (C) Quantification of MOR-mCherry expression in S1 comparing female (n = 10 sections, 3 mice) and male mice (n = 12 sections, 3 mice). Two-way mixed ANOVA $F(5,117) = 5.42$, $P < 0.001$. (D) Quantification of MOR-mCherry expression in male and female ACC. Two-way mixed ANOVA $F(4,100) = 5.51$, $P < 0.001$. Wilcoxon signed rank test. Data are presented as mean ± SEM. *$P <$ 0.05, **$P < 0.01$, ***$P < 0.001$. MORs, mu opioid receptors.

Females also had higher levels of MOR-mCherry+ neurons than males in S1 L2/3 (2.7% ± 0.4% vs 1.5% ± 0.1%, $P < 0.01$), S1 L4 (1.9% ± 0.3% vs 1% ± 0.1%, $P < 0.05$), and S1 L6a (4.9% ± 0.5% vs 3.4% ± 0.5%, $P < 0.05$). In ACC, the greatest sex differences were found in L6b, where females had significantly higher proportions of MOR-mCherry+ neurons (13.1% of total neurons ± 1.8%) than males (5.6% ± 0.8%) ($P < 0.01$). Females also had higher levels of MOR-mCherry than males in ACC L2/3 (2.7% ± 0.4% vs 1.7% ± 0.2%, $P < 0.05$), in ACC L5 (6.9% ± 0.9% vs 3.7% ± 0.2%, $P < 0.01$), in ACC L6a (5.1% ± 0.7% vs 2.7% ± 0.2%, $P < 0.01$) (**Fig. 6D**). A larger sample size will be needed to determine differences in subpopulation of neurons underlying these sex differences in MOR expression.

4. Discussion

4.1. Distinct electrophysiological properties of mu opioid receptor–expressing neurons in anterior cingulate cortex and S1

Our initial experiments suggested that blind recordings in wild-type mice were unsuited for investigation of MOR-expressing neurons. Using the *Oprm1*$^{mCherry/mCherry}$ mouse line, we found that MOR-expressing neurons in ACC had interneuron-like firing patterns, whereas the recorded MOR-negative neurons more often displayed pyramidal neuron-like firing. In our immunohistochemistry experiments, we found that the population of MOR-expressing neurons in ACC are both excitatory (SATB2+) and inhibitory. The electrophysiology recordings could only be performed on the brightest mCherry-expressing fluorescent neurons (see Materials and Methods). For this reason, further IHC experiments were conducted to characterize all the subpopulations of MOR-expressing neurons. It has been shown that there are few excitatory interneurons in the cortex, most of which residing in layer 4, as such it is unlikely that the interneuron-like firing pattern corresponds to SATB2+ neurons.[18] In contrast to the ACC, we found that S1 MOR-expressing neurons more often displayed pyramidal neuron-like firing patterns.

4.2. Mu opioid receptor expression in output layers 5 and 6b

In ACC and S1, the highest levels of MOR were found in L6b. L6b integrates information from long-range intracortical pathways and projects to the thalamus and other cortical areas.[55] Interestingly, we found no significant differences in the subtypes of neurons expressing MOR in between ACC and S1 for L6b. L6b MOR-expressing neurons were primarily excitatory neurons; this suggests that MOR activation would result in decreased output of ACC and S1. Inhibition of ACC L5 pyramidal neurons projecting to the spinal cord is analgesic.[9] This suggests that MOR activation in ACC L5 pyramidal neurons could be analgesic. Similarly, S1 L5 pyramidal neurons also project directly to the spinal cord,[31] and MOR activation could be analgesic. For L6b and L5, the proportion of MOR-expressing neurons was significantly greater in S1 than in ACC. It is possible that this difference parallels the small receptive field size of S1 pain-responsive neurons, whereas the ACC pain-responsive neurons have large or "whole-body" receptive fields.[53]

4.3. Increased prevalence of mu opioid receptors on SOM interneurons in anterior cingulate cortex compared with S1

Opioid analgesia causes increased activity in ACC and PAG, which may allow for activation of the descending modulatory pain pathway.[50] In line with this study, we found substantial expression of MOR on SOM interneurons in the ACC, which could allow for disinhibition of pyramidal neurons.[23] Specifically, for L1, L2/3, and L5, we found an increased prevalence of MOR/SOM co-expression in ACC compared with S1. Our study did not investigate whether inhibition of MOR/SOM co-expressing neurons in ACC results in activation of the PAG. More research will be necessary to discern the role of MOR-expressing SOM interneurons and downstream effects of cortical disinhibition in both ACC and S1.

4.4. Opioid receptor subtypes by layer in anterior cingulate cortex and S1

In the ACC, delta opioid receptors (DORs) are predominantly expressed on different neurons than MORs, and DORs are more densely located in L2/3.[51] Furthermore, in ACC L5, DORs are expressed on PV interneurons.[3] In line with this research, we found minimal expression of MOR in L2/3 and minimal PV/MOR co-expression. L2/3 and L5 pyramidal neurons function differently in information processing.[38] L2/3 is thought to convey spike-encoded information (sparse-coding) to other cortical areas, meaning a large number of neurons are required but only few neurons are active at a time to encode the stimulus.[15] This sparse-coding may require increased feedforward inhibition by PV interneurons to prevent loss of signal as information reaches higher hierarchical levels.[15,18] In contrast, L5 uses dense coding, meaning a relatively large group of neurons respond to a stimulus and have higher firing rates to allow the transmission of information to more distant targets.[19] This could suggest a modulatory role for DORs expressed at higher levels in L2/3 in PV interneurons, as this layer may require more time-sensitive activity because of the spike-encoded method of information processing. In contrast, L5 may rely on MOR inhibition on SOM interneurons, which efficiently modulate the dense coding method of information processing.[28] Interestingly, we found that in L5, S1 had greater MOR/PV co-expression compared with ACC, suggesting that DOR expression could also vary between cortical areas. Kappa and nociceptin opioid receptors are expressed in ACC and S1 too; however, more research is needed to resolve their precise cellular localizations and functions.[29,33,34] We focused this study on identifying the neuronal subtypes expressing MOR. However, as MOR has been reported to be expressed in astrocytes and microglia,[32,39,52] its role in glial cells in ACC and S1 will also remain to be investigated.

4.5. Acute and chronic pain processing in anterior cingulate cortex and S1

In the ACC, the proportion of neurons activated during acute pain could range from 14% to 40% of pyramidal neurons.[21,48] It is currently unknown which proportion of neurons in S1 are activated during acute pain and how this proportion compares with that found in the ACC. We found that the MOR-expressing neurons represent roughly 2% to 37% of total neurons. This suggests that MOR-expressing neuronal populations could represent a subset of the acute pain activated population. More research is needed confirm whether MOR-expressing neurons are responsive to acute pain. Chronic neuropathic pain results in changes in cortical function in both ACC and S1, and researchers consistently find increased excitation of pyramidal neurons.[4,10,12,26,27,46] The increase in pyramidal neuron excitation seems to be consistent in L2/3 and L5 and is likely not restricted to pyramidal neurons activated during acute pain. As such, this

suggests that MOR-expressing pyramidal neurons experience an increase in excitability in chronic neuropathic pain. Finally, decreased activity of interneurons in ACC and S1 in chronic neuropathic pain has also been reported,[4,10] indicating that MOR-expressing interneurons could play an important role in both acute and chronic pain conditions.

4.6. Role of anterior cingulate cortex, ventral tegmental area, and nucleus accumbens in pain relief

Navratilova and collaborators reported that direct injection of morphine into the ACC of rats with neuropathic pain is analgesic.[40] Furthermore, injection of the opioid antagonist naloxone in the ACC reversed the analgesia induced by injection of nonopioid analgesics. This suggests that endogenous opioids in the ACC are required for pain relief.[41] The ACC projects to the ventral tegmental area (VTA) and nucleus accumbens (NAc). Reward from pain relief is accompanied by dopamine (DA) release in the NAc and conditioned place preference to the paired chamber.[17,24,27,40] MOR activation on SOM interneurons could result in disinhibition of ACC L5 pyramidal neurons projecting to VTA, increased activity of VTA DAergic neurons, and DA release into the NAc, which would be analgesic.[40] The ACC projects directly to the NAc, but it is unclear onto which neuron types. Within the NAc, there are GABAergic neurons expressing either dopamine receptors D1 (Gs coupled) or D2 (Gi coupled) that promote reward and aversion pathways, respectively.[25,49] Mu opioid receptor activation on pyramidal neurons projecting onto NAc D2-expressing neurons could decrease the affective component of pain.

4.7. Cortical layer expression of endogenous opioid peptides

Endogenous opioid peptides are located throughout the ACC and S1.[30] The gene encoding enkephalins, preproenkephalin (*Penk*), is expressed at higher levels in L2/3, L6a, and L6b. The precursor for dynorphin, preprodynorphin (*Pdyn*), is expressed in L2/3 and L5.[30] Interestingly, *Pdyn* mRNA is highly expressed by SOM interneurons and moderately expressed by pyramidal neurons in L6b, as well as in VIP interneurons.[54] Therefore, L2/3 and L5 MOR/SOM co-expressing interneurons could release dynorphins, and it is possible that L6b MOR-expressing pyramidal neurons could also release dynorphins. In addition, MORs located more densely in L5 and in L6b could be involved in response to dynorphins and enkephalins, respectively.

4.8. Sex differences in pain and cortical mu opioid receptor expression

Zubieta et al. reported that females have higher MOR levels compared with males in several brain areas, including the ACC; however, no sex differences were reported in S1.[57] We found that in both ACC and S1, female mice have more MOR-expressing neurons than male mice. Qualitatively, we observed similar distribution of MOR on neuronal subtypes, with both males and females having greater MOR/SOM co-expression in ACC compared with S1, and more excitatory neurons expressing MOR in S1. More research focusing on sex differences will be needed to determine why higher levels of MOR in females compared with males are related to decreased effectiveness of opioid analgesics.[32]

Conflict of interest statement

The authors have no conflicts of interest to declare.

Acknowledgments

This work was supported by a Canadian Institutes of Health Research (CIHR) grant to PS (PJT-153098) and by the New York Stem Cell Foundation (GS). GS is a Robertson Investigator of the New York Stem Cell Foundation. MZ, BS, and SL held PhD student fellowships from the Louise and Alan Edwards Foundation. The authors are grateful to Melina Jaramillo Garcia in the Molecular and Cellular Imaging platform of the Douglas Research Institute for technical help and to Dr. Thomas Stroh and Dr. Liliana Pedraza at the Montreal Neurological Institute for expert advice and access to the Neuro Microscopy Imaging Centre.

Appendix A. Supplemental digital content

Supplemental digital content associated with this article can be found online at http://links.lww.com/PAIN/B700.

Article history:
Received 14 April 2022
Received in revised form 24 June 2022
Accepted 22 July 2022
Available online 16 August 2022

References

[1] Al-Hasani R, Bruchas MR. Molecular mechanisms of opioid receptor-dependent signaling and behavior. Anesthesiology 2011;115:1363–81.
[2] Bailly J, Del Rossi N, Runtz L, Li JJ, Park D, Scherrer G, Tanti A, Birling MC, Darcq E, Kieffer BL. Targeting morphine-responsive neurons: generation of a knock-in mouse line expressing cre recombinase from the mu-opioid receptor gene locus. eNeuro 2020;7:ENEURO.0433-19.2020.
[3] Birdsong WT, Jongbloets BC, Engeln KA, Wang D, Scherrer G, Mao T. Synapse-specific opioid modulation of thalamo-cortico-striatal circuits. eLife 2019;8:e45146.
[4] Blom SM, Pfister J-P, Santello M, Senn W, Nevian T. Nerve injury-induced neuropathic pain causes disinhibition of the anterior cingulate cortex. J Neurosci 2014;34:5754–64.
[5] Bogovic JA, Hanslovsky P, Wong A, Saalfeld S. Robust registration of calcium images by learned contrast synthesis. IEEE 13th International Symposium on Biomedical Imaging (ISBI). Prague, Czech Republic: IEEE, 2016; 1123–6. doi: 10.1109/ISBI.2016.7493463.
[6] Britanova O, de Juan Romero C, Cheung A, Kwan KY, Schwark M, Gyorgy A, Vogel T, Akopov S, Mitkovski M, Agoston D, Šestan N, Molnár Z, Tarabykin V. Satb2 is a postmitotic determinant for upper-layer neuron specification in the neocortex. Neuron 2008;57:378–92.
[7] Bushnell MC, Duncan GH, Hofbauer RK, Ha B, Chen J-I, Carrier B. Pain perception: is there a role for primary somatosensory cortex?. Proc Natl Acad Sci 1999;96:7705–9.
[8] Chan KY, Jang MJ, Yoo BB, Greenbaum A, Ravi N, Wu WL, Sánchez-Guardado L, Lois C, Mazmanian SK, Deverman BE, Gradinaru V. Engineered AAVs for efficient noninvasive gene delivery to the central and peripheral nervous systems. Nat Neurosci 2017;20:1172–9.
[9] Chen T, Taniguchi W, Chen QY, Tozaki-Saitoh H, Song Q, Liu R-H, Koga K, Matsuda T, Kaito-Sugimura Y, Wang J, Li ZH, Lu YC, Inoue K, Tsuda M, Li YQ, Nakatsuka T, Zhuo M. Top-down descending facilitation of spinal sensory excitatory transmission from the anterior cingulate cortex. Nat Commun 2018;9:1886.
[10] Cichon J, TJJ Blanck, Gan W-B, Yang G. Activation of cortical somatostatin interneurons prevents the development of neuropathic pain. Nat Neurosci 2017;20:1122–32.
[11] Coghill RC, Sang CN, JMa Maisog, Iadarola MJ. Pain intensity processing within the human brain: a bilateral, distributed mechanism. J Neurophysiol 1999;82:1934–43.
[12] Cordeiro Matos S, Zamfir M, Longo G, Ribeiro-da-Silva A, Séguéla P. Noradrenergic fiber sprouting and altered transduction in neuropathic

prefrontal cortex. Brain Struct Funct 2017. doi: 10.1007/s00429-017-1543-7
[13] Corder G, Castro DC, Bruchas MR, Scherrer G. Endogenous and exogenous opioids in pain. Annu Rev Neurosci 2018;41:453–73.
[14] Corder G, Tawfik VL, Wang D, Sypek EI, Low SA, Dickinson JR, Sotoudeh C, Clark JD, Barres BA, Bohlen CJ, Scherrer G. Loss of μ opioid receptor signaling in nociceptors, but not microglia, abrogates morphine tolerance without disrupting analgesia. Nat Med 2017;23:164–73.
[15] D'Souza RD, Burkhalter AA. Laminar organization for selective cortico-cortical communication. Front Neuroanat 2017;11:71.
[16] Erbs E, Faget L, Scherrer G, Matifas A, Filliol D, Vonesch JL, Koch M, Kessler P, Hentsch D, Birling M-C, Koutsourakis M, Vasseur L, Veinante P, Kieffer BL, Massotte D. A mu–delta opioid receptor brain atlas reveals neuronal co-occurrence in subcortical networks. Brain Struct Funct 2015;220:677–702.
[17] Fillinger C, Yalcin I, Barrot M, Veinante P. Afferents to anterior cingulate areas 24a and 24b and midcingulate areas 24a′ and 24b′ in the mouse. Brain Struct Funct 2017;222:1509–32.
[18] Fishell G, Rudy B. Mechanisms of inhibition within the telencephalon: "where the wild things are. Annu Rev Neurosci 2011;34:535–67.
[19] Harris KD, Mrsic-Flogel TD. Cortical connectivity and sensory coding. Nature 2013;503:51–8.
[20] van Heukelum S, Mars RB, Guthrie M, Buitelaar JK, Beckmann CF, Tiesinga PHE, Vogt BA, Glennon JC, Havenith MN. Where is cingulate cortex? A cross-species view. Trends Neurosciences 2020;43:285–99.
[21] Káradóttir R, Attwell D. Combining patch-clamping of cells in brain slices with immunocytochemical labeling to define cell type and developmental stage. Nat Protoc 2006;1:1977–86.
[22] Kasanetz F, Acuña MA, Nevian T. Anterior cingulate cortex, pain perception, and pathological neuronal plasticity during chronic pain. The Neurobiology, Physiology, and Psychology of Pain. Elsevier, 2022; 193–202. doi: 10.1016/B978-0-12-820589-1.00018-X
[23] Kepecs A, Fishell G. Interneuron cell types are fit to function. Nature 2014; 505:318–26.
[24] Kieffer BL. Opioids: first lessons from knockout mice. Trends Pharmacol Sci 1999;20:19–26.
[25] Kimmey BA, McCall NM, Wooldridge LM, Satterthwaite TD, Corder G. Engaging endogenous opioid circuits in pain affective processes. J Neurosci Res 2020:jnr.24762.
[26] Lammel S, Lim BK, Ran C, Huang KW, Betley MJ, Tye KM, Deisseroth K, Malenka RC. Input-specific control of reward and aversion in the ventral tegmental area. Nature 2012;491:212–17.
[27] Lançon K, Navratilova E, Porreca F, Séguéla P. Dopaminergic inhibition of pyramidal cells in anterior cingulate cortex is defective in chronic neuropathic pain. SSRN J 2020. doi: 10.2139/ssrn.3613762
[28] Larkum M. A cellular mechanism for cortical associations: an organizing principle for the cerebral cortex. Trends Neurosciences 2013;36:141–51.
[29] Lee S, Hjerling-Leffler J, Zagha E, Fishell G, Rudy B. The largest group of superficial neocortical GABAergic interneurons expresses ionotropic serotonin receptors. J Neurosci 2010;30:16796–808.
[30] Lein ES, Hawrylycz MJ, Ao N, Ayres M, Bensinger A, Bernard A, Boe AF, Boguski MS, Brockway KS, Byrnes EJ, Chen L, Chen L, Chen TM, Chi Chin M, Chong J, Crook BE, Czaplinska A, Dang CN, Datta S, Dee NR, Desaki AL, Desta T, Diep E, Dolbeare TA, Donelan MJ, Dong HW, Dougherty JG, Duncan BJ, Ebbert AJ, Eichele G, Estin LK, Faber C, Facer BA, Fields R, Fischer SR, Fliss TP, Frensley C, Gates SN, Glattfelder KJ, Halverson KR, Hart MR, Hohmann JG, Howell MP, Jeung DP, Johnson RA, Karr PT, Kawal R, Kidney JM, Knapik RH, Kuan CL, Lake JH, Laramee AR, Larsen KD, Lau C, Lemon TA, Liang AJ, Liu Y, Luong LT, Michaels J, Morgan JJ, Morgan RJ, Mortrud MT, Mosqueda NF, Ng LL, Ng R, Orta GJ, Overly CC, Pak TH, Parry SE, Pathak SD, Pearson OC, Puchalski RB, Riley ZL, Rockett HR, Rowland SA, Royall JJ, Ruiz MJ, Sarno NR, Schaffnit K, Shapovalova NV, Sivisay T, Slaughterbeck CR, Smith SC, Smith KA, Smith BI, Sodt AJ, Stewart NN, Stumpf K-R, Sunkin SM, Sutram M, Tam A, Teemer CD, Thaller C, Thompson CL, Varnam LR, Visel A, Whitlock RM, Wohnoutka PE, Wolkey CK, Wong VY, Wood M, Yaylaoglu MB, Young RC, Youngstrom BL, Feng Yuan X, Zhang B, Zwingman TA, Jones AR. Genome-wide atlas of gene expression in the adult mouse brain. Nature 2007;445:168–76.
[31] Liu Y, Latremoliere A, Li X, Zhang Z, Chen M, Wang X, Fang C, Zhu J, Alexandre C, Gao Z, Chen B, Ding X, Zhou J-Y, Zhang Y, Chen C, Wang KH, Woolf CJ, He Z. Touch and tactile neuropathic pain sensitivity are set by corticospinal projections. Nature 2018;561:547–50.
[32] Loyd DR, Murphy AZ. The neuroanatomy of sexual dimorphism in opioid analgesia. Exp Neurol 2014;259:57–63.
[33] Maduna T, Audouard E, Dembélé D, Mouzaoui N, Reiss D, Massotte D, Gaveriaux-Ruff C. Microglia express mu opioid receptor: insights from transcriptomics and fluorescent reporter mice. Front Psychiatry 2019;9:726.
[34] Mansour A, Fox CA, Burke S, Meng F, Thompson RC, Akil H, Watson SJ. Mu, delta, and kappa opioid receptor mRNA expression in the rat CNS: an in situ hybridization study. J Comp Neurol 1994;350:412–38.
[35] Mansour A, Khachaturian H, Lewis ME, Akil H, Watson SJ. Autoradiographic differentiation of mu, delta, and kappa opioid receptors in the rat forebrain and midbrain. J Neurosci 1987;7:2445–64.
[36] Melzack R, Casey KL. Sensory,Motivational,and Central Control Determinants of Pain. The Skin Senses. Charles C Thomas. Springfield, IL, 1968; 423–39.
[37] Mogil JS, Bailey AL. Sex and gender differences in pain and analgesia. Progress in Brain Research. Vol 186. Elsevier, 2010; 140–57. doi: 10.1016/B978-0-444-53630-3.00009-9
[38] Naka A, Adesnik H. Inhibitory circuits in cortical layer 5. Front Neural Circuits 2016;10. doi: 10.3389/fncir.2016.00035
[39] Nam M-H, Han K-S, Lee J, Won W, Koh W, Bae JY, Woo J, Kim J, Kwong E, Choi T-Y, Chun H, Lee SE, Kim S-B, Park KD, Choi S-Y, Bae YC, Lee CJ. Activation of astrocytic μ-opioid receptor causes conditioned place preference. Cell Rep 2019;28:1154–66.e5.
[40] Navratilova E, Atcherley CW, Porreca F. Brain circuits encoding reward from pain relief. Trends Neurosciences 2015;38:741–50.
[41] Navratilova E, Xie JY, Meske D, Qu C, Morimura K, Okun A, Arakawa N, Ossipov M, Fields HL, Porreca F. Endogenous opioid activity in the anterior cingulate cortex is required for relief of pain. J Neurosci 2015;35:7264–71.
[42] Pietzsch T, Saalfeld S, Preibisch S, Tomancak P. BigDataViewer: visualization and processing for large image data sets. Nat Methods 2015;12:481–3.
[43] Price DD, Von der Gruen A, Miller J, Rafii A, Price C. A psychophysical Anal morphine analgesia. PAIN 1985;22:261–9.
[44] Rainville P. Pain affect encoded in human anterior cingulate but not somatosensory cortex. Science 1997;277:968–71.
[45] Santello M, Nevian T. Dysfunction of cortical dendritic integration in neuropathic pain reversed by serotoninergic neuromodulation. Neuron 2015;86:233–46.
[46] Scherrer G, Imamachi N, Cao YQ, Contet C, Mennicken F, O'Donnell D, Kieffer BL, Basbaum AI. Dissociation of the opioid receptor mechanisms that control mechanical and heat pain. Cell 2009;137:1148–59.
[47] Singh A, Patel D, Li A, Hu L, Zhang Q, Liu Y, Guo X, Robinson E, Martinez E, Doan L, Rudy B, Chen ZS, Wang J. Mapping cortical integration of sensory and affective pain pathways. Curr Biol 2020;30:1703–15.e5.
[48] Tan LL, Kuner R. Neocortical circuits in pain and pain relief. Nat Rev Neurosci 2021;22:458–71.
[49] Volkow ND, McLellan AT. Opioid abuse in chronic pain—misconceptions and mitigation strategies. N Engl J Med 2016;374:1253–63.
[50] Wagner KJ, Sprenger T, Kochs EF, Tölle TR, Valet M, Willoch F. Imaging human cerebral pain modulation by dose-dependent opioid analgesia. Anesthesiology 2007;106:548–56.
[51] Wang D, Tawfik VL, Corder G, Low SA, François A, Basbaum AI, Scherrer G. Functional divergence of delta and mu opioid receptor organization in CNS pain circuits. Neuron 2018;98:90–108.e5.
[52] Watkins LR, Hutchinson MR, Rice KC, Maier SF. The "toll" of opioid-induced glial activation: improving the clinical efficacy of opioids by targeting glia. Trends Pharmacol Sci 2009;30:581–91.
[53] Yamamura H, Iwata K, Tsuboi Y, Toda K, Kitajima K, Shimizu N, Nomura H, Hibiya J, Fujita S, Sumino R. Morphological and electrophysiological properties of ACCx nociceptive neurons in rats. Brain Res 1996;735: 83–92.
[54] Zeisel A, Muñoz-Manchado AB, Codeluppi S, Lönnerberg P, La Manno G, Juréus A, Marques S, Munguba H, He L, Betsholtz C, Rolny C, Castelo-Branco G, Hjerling-Leffler J, Linnarsson S. Cell types in the mouse cortex and hippocampus revealed by single-cell RNA-seq. Science 2015;347:1138–42.
[55] Zolnik TA, Ledderose J, Toumazou M, Trimbuch T, Oram T, Rosenmund C, Eickholt BJ, Sachdev RNS, Larkum ME. Layer 6b is driven by intracortical long-range projection neurons. Cell Rep 2020;30:3492–505. e5.
[56] Zubieta J-K. Regional mu opioid receptor regulation of sensory and affective dimensions of pain. Science 2001;293:311–15.
[57] Zubieta J-K, Dannals RF, Frost JJ. Gender and age influences on human brain mu-opioid receptor binding measured by PET. AJP 1999;156:842–8.